http://www.applmathmech.cn

# 含切口的压电准晶组合结构界面断裂分析的辛-等几何耦合方法*

杨震霆, 王雅静, 聂雪阳, 徐新生, 周震寰

(大连理工大学 工程力学系 工业装备结构分析优化与 CAE 软件全国重点实验室, 辽宁 大连 116024)

**摘要:** 发展了一种适用于含有切口的压电准晶/压电晶体/弹性体三材料组合结构界面断裂问题的高精度的半数值半解析方法.首先,通过引入 Hamilton 体系建立了三材料组合结构的 Hamilton 对偶方程,将原问题在传统 Lagrange 体系下的高阶偏微分控制方程转化为低阶常微分方程组.其次,通过分离变量法求解问题对应的辛本征值和本征解,将各物理场变量利用辛级数展开形式表示.最后,将辛级数与等几何分析方法相结合,获得了辛-等几何耦合列式,直接求得切口尖端附近奇异物理场及其强度因子的解析表达式.

**关 键 词:** 准晶体; 压电材料; 等几何分析; Hamilton 体系; V 形切口; 界面断裂

**中图分类号:** O346　　**文献标志码:** A　　DOI: 10.21656/1000-0887.440247

# Symplectic Isogeometric Analysis Coupling Method for Interfacial Fracture of Piezoelectric Quasicrystal Composites With Notches

YANG Zhenting, WANG Yajing, NIE Xueyang, XU Xinsheng, ZHOU Zhenhuan

(*State Key Laboratory of Structural Analysis, Optimization and CAE Software for Industrial Equipment, Department of Engineering Mechanics, Dalian University of Technology, Dalian, Liaoning* 116024, *P.R.China*)

**Abstract**: A high-precision semi numerical and semi analytical method for interfacial fracture problem of piezoelectric quasicrystals (PQCs)/piezoelectric crystals (PZCs)/elastic material composites with notches was developed. Firstly, the Hamiltonian system was introduced and the Hamiltonian dual equations for the 3-material composite were formulated. The higher order partial differential governing equations were transformed into a set of ordinary differential equations. Secondly, the symplectic eigenvalues and eigensolutions were obtained through separation of variables. The physical quantities were expressed with the expansion of symplectic series. Finally, a symplectic isogeometric analysis (IGA) coupling equation was derived through combination of the symplectic series and the IGA. The analytical expressions of the physical quantities near the notch tip and the intensity factors were derived.

**Key words**: quasicrystal; piezoelectric material; isogeometric analysis; Hamiltonian system; V notch; interfacial fracture

* **收稿日期:** 2023-08-17; **修订日期:** 2023-10-12

**基金项目:** 辽宁省自然科学基金(2023-MS-118)

**作者简介:** 杨震霆(1994—),男,博士生(E-mail: zhentingyang@outlook.com);
周震寰(1983—),男,教授,博士(通讯作者. E-mail: zhouzh@dlut.edu.cn).

**引用格式:** 杨震霆, 王雅静, 聂雪阳, 徐新生, 周震寰. 含切口的压电准晶组合结构界面断裂分析的辛-等几何耦合方法[J]. 应用数学和力学, 2024, **45**(2): 144-154.

# 0 引　　言

1983 年,诺贝尔奖获得者 Shechtman 教授首次在急速冷却的铝锰合金中发现了一种介于晶体与非晶体之间的物质——准晶体(QC).该类物质由于特殊的微观结构,表现出诸多优良的属性,如隔热、耐腐蚀、耐磨等,可用于制备太阳能选择吸收器、储氢材料等,在航空航天领域和新能源领域具有广阔的应用前景.但是,准晶体为脆性材料,自身极易发生断裂失效,需要与其他材料组合使用.然而,由于材料失配问题,不同材料的界面处不可避免地会出现界面断裂.因此,研究准晶体组合结构的界面断裂问题具有重要的实际意义.

目前,准晶体/压电准晶体(PQC)的断裂力学研究已经受到了学术界的广泛关注.基于准晶体的弹性理论[1],Fan(范天佑)等首次研究了准晶体中的 Griffith 裂纹[2-3].此后,研究者们进一步深入研究了准晶体线弹性断裂问题[4-13].在压电准晶体断裂方面:Jiang 和 Liu[14]研究了含有 V 形切口的一维六方压电准晶体断裂问题,并推导了应力强度因子的解析解;Li 等[15]采用奇异积分方程研究了横观各向同性压电准晶体圆柱壳的断裂问题;Zhou 和 Li[16]考虑了压电准晶体中的半渗透裂纹并求解了应力强度因子;Zhao 等[17-18]发展了一种扩展位移不连续边界元法,研究了双压电准晶体材料的界面断裂问题;Hu 等[19]研究了双压电准晶体材料中的双界面裂纹.

上述研究工作主要集中于单一准晶体/压电准晶体断裂问题,解析分析主要基于单变量的 Lagrange 求解系统,需要根据边界条件构造假设函数,因此大部分研究工作为无限大或半无限大的模型.此外,目前还没有针对含有切口的压电准晶体/压电晶体/弹性体多材料界面反平面断裂问题的相关研究.为解决上述问题,本文将辛方法与等几何方法[20]相结合,发展了一种适用于压电准晶体/压电晶体/弹性体多材料组合结构反平面界面断裂问题的辛-等几何耦合方法.辛方法[21]是钟万勰院士首次提出的一种全新的解析求解方法,该方法无需构造假设函数,是一种直接理性的求解方法,目前已广泛应用于多场耦合材料力学问题和断裂力学领域.相比传统方法,提出的辛-等几何耦合方法主要具有以下三方面优势:① 无需切口尖端的控制点加密,节省了大量计算资源; ② 无需后处理,直接获得切口尖端附近的物理场和强度因子解析表达式,计算精度大幅提高; ③ 可以避免复杂的网格剖分过程.

# 1 压电准晶体/压电晶体/弹性体的辛体系

## 1.1 基本模型

含 V 形切口的三材料组合结构如图 1 所示,为了研究切口在不同材料界面的情况,这里考虑 3 种情况:① 切口位于压电准晶体和弹性体之间,即 $M_1$ 为压电准晶,$M_2$ 为压电晶体(PZC),$M_3$ 为弹性体(情况 1); ② 切口位于压电晶体和弹性体之间,即 $M_1$ 为压电晶体,$M_2$ 为压电准晶,$M_3$ 为弹性体(情况 2); ③ 切口位于压电准晶体和压电晶体之间,即 $M_1$ 为压电准晶,$M_2$ 为弹性体,$M_3$ 为压电晶体(情况 3).以切口尖端为原点,以上切口面为 $x$ 轴和极轴建立直角坐标系 $(x,y)$ 和柱坐标系 $(r,\theta,z)$,以不同材料界面分别建立两个子柱坐标系 $(r_1,\theta_1,z_1)$ 和 $(r_2,\theta_2,z_2)$.

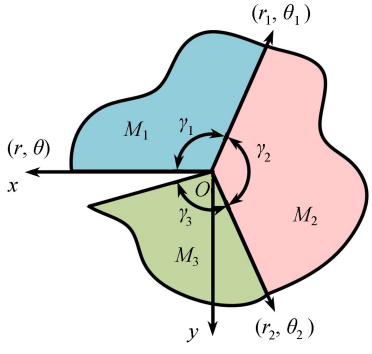


**图 1**　含切口的三材料组合结构

Fig. 1　The 3-material composite with a notch

## 1.2 Hamilton 对偶方程

由文献[22-23],三种材料反平面问题的应变能密度和对应的 Lagrange 密度函数为:

应变能密度

$$\boldsymbol{\Pi}^{(\mathrm{PQC})}=\frac{1}{2}\boldsymbol{\sigma}^{(\mathrm{PQC})}\boldsymbol{\gamma}^{(\mathrm{PQC})}+\frac{1}{2}\boldsymbol{H}^{(\mathrm{PQC})}\boldsymbol{\omega}^{(\mathrm{PQC})}-\frac{1}{2}\boldsymbol{E}^{(\mathrm{PQC})}\boldsymbol{D}^{(\mathrm{PQC})}-\{u_z^{(\mathrm{PQC})},w_z^{(\mathrm{PQC})},\varphi^{(\mathrm{PQC})}\}\{T_\sigma^{(\mathrm{PQC})},T_H^{(\mathrm{PQC})},T_D^{(\mathrm{PQC})}\}^{\mathrm{T}},\tag{1}$$

$$\Pi^{(\mathrm{PZC})}=\frac{1}{2}\boldsymbol{\sigma}^{(\mathrm{PZC})}\boldsymbol{\gamma}^{(\mathrm{PZC})}-\frac{1}{2}\boldsymbol{E}^{(\mathrm{PZC})}\boldsymbol{D}^{(\mathrm{PZC})}-\{u_z^{(\mathrm{PZC})},\varphi^{(\mathrm{PZC})}\}\{T_\sigma^{(\mathrm{PZC})},T_D^{(\mathrm{PZC})}\}^{\mathrm{T}},\tag{2}$$

$$\Pi^{(\mathrm{e})}=\frac{1}{2}\boldsymbol{\sigma}^{(\mathrm{e})}\boldsymbol{\gamma}^{(\mathrm{e})}-u_z^{(\mathrm{e})}T_\sigma^{(\mathrm{e})};\tag{3}$$

Lagrange 密度函数

$$\begin{aligned}L^{(\mathrm{PQC})}=&\frac{1}{2}C_{44}^{(\mathrm{PQC})}\left(\frac{\partial u_z^{(\mathrm{PQC})}}{\partial\theta}\right)^2+R_3^{(\mathrm{PQC})}\frac{\partial w_z^{(\mathrm{PQC})}}{\partial\theta}\frac{\partial u_z^{(\mathrm{PQC})}}{\partial\theta}+e_{15}^{(\mathrm{PQC})}\frac{\partial\varphi^{(\mathrm{PQC})}}{\partial\theta}\frac{\partial u_z^{(\mathrm{PQC})}}{\partial\theta}+\\&\frac{1}{2}C_{44}^{(\mathrm{PQC})}(\dot{u}_z^{(\mathrm{PQC})})^2+R_3^{(\mathrm{PQC})}\dot{u}_z^{(\mathrm{PQC})}\dot{w}_z^{(\mathrm{PQC})}+e_{15}^{(\mathrm{PQC})}\dot{u}_z^{(\mathrm{PQC})}\dot{\varphi}^{(\mathrm{PQC})}+d_{15}^{(\mathrm{PQC})}\frac{\partial\varphi^{(\mathrm{PQC})}}{\partial\theta}\frac{\partial w_z^{(\mathrm{PQC})}}{\partial\theta}-\\&\frac{1}{2}\lambda_{11}^{(\mathrm{PQC})}\left(\frac{\partial\varphi^{(\mathrm{PQC})}}{\partial\theta}\right)^2+\frac{1}{2}K_2^{(\mathrm{PQC})}\left(\frac{\partial w_z^{(\mathrm{PQC})}}{\partial\theta}\right)^2+\frac{1}{2}K_2^{(\mathrm{PQC})}(\dot{w}_z^{(\mathrm{PQC})})^2+\\&d_{15}^{(\mathrm{PQC})}\dot{\varphi}\dot{w}_z^{(\mathrm{PQC})}-\frac{1}{2}\lambda_{11}^{(\mathrm{PQC})}(\dot{\varphi}^{(\mathrm{PQC})})^2,\end{aligned}\tag{4}$$

$$\begin{aligned}L^{(\mathrm{PZC})}=&\frac{1}{2}C_{44}^{(\mathrm{PZC})}\left(\frac{\partial u_z^{(\mathrm{PZC})}}{\partial\theta}\right)^2+R_3^{(\mathrm{PZC})}\frac{\partial w_z^{(\mathrm{PZC})}}{\partial\theta}\frac{\partial u_z^{(\mathrm{PZC})}}{\partial\theta}+\frac{1}{2}C_{44}^{(\mathrm{PZC})}(\dot{u}_z^{(\mathrm{PZC})})^2+\\&R_3^{(\mathrm{PZC})}\dot{u}_z^{(\mathrm{PZC})}\dot{w}_z^{(\mathrm{PZC})}+\frac{1}{2}K_2^{(\mathrm{PZC})}\left(\frac{\partial w_z^{(\mathrm{PZC})}}{\partial\theta}\right)^2+\frac{1}{2}K_2^{(\mathrm{PZC})}(\dot{w}_z^{(\mathrm{PZC})})^2,\end{aligned}\tag{5}$$

$$L^{(\mathrm{e})}=\frac{1}{2}C_{44}^{(\mathrm{e})}\left(\frac{\partial u_z^{(\mathrm{e})}}{\partial\theta}\right)^2,\tag{6}$$

其中上标(PQC)、(PZC)、(e)分别代表压电准晶体、压电晶体和弹性体材料; $\boldsymbol{\sigma}^{(i)}=\{\sigma_{z\theta}^{(i)},\sigma_{zr}^{(i)}\}$ 和 $\boldsymbol{\gamma}^{(i)}=\{\gamma_{z\theta}^{(i)},\gamma_{zr}^{(i)}\}^{\mathrm{T}}$ 为声子场的应力和应变, $\boldsymbol{H}^{(i)}=\{H_{z\theta}^{(i)},H_{zr}^{(i)}\}$ 和 $\boldsymbol{\omega}^{(i)}=\{\omega_{z\theta}^{(i)},\omega_{zr}^{(i)}\}^{\mathrm{T}}$ 为相位子场的应力和应变, $\boldsymbol{D}^{(i)}=\{D_\theta^{(i)},D_r^{(i)}\}$ 和 $\boldsymbol{E}^{(i)}=\{E_\theta^{(i)},E_r^{(i)}\}^{\mathrm{T}}$ 为电位移和电场强度; $C_{44}^{(i)}$ 为声子场弹性模量, $K_2^{(i)}$ 为相位子场弹性模量, $R_3^{(i)}$ 为声子场-相位子场耦合系数, $e_{15}^{(i)}$ 和 $d_{15}^{(i)}$ 分别为声子场和相位子场压电常数, $\lambda_{11}^{(i)}$ 为介电常数; $(\dot{})=\partial(\,)/\partial\xi$, $\xi=\ln r$ 为广义坐标.

引入广义位移向量:

$$\boldsymbol{q}^{(\mathrm{PQC})}=\{u_z^{(\mathrm{PQC})},w_z^{(\mathrm{PQC})},\varphi^{(\mathrm{PQC})}\}^{\mathrm{T}},\ \boldsymbol{q}^{(\mathrm{PZC})}=\{u_z^{(\mathrm{PZC})},w_z^{(\mathrm{PZC})}\}^{\mathrm{T}},\ q^{(\mathrm{e})}=u_z^{(\mathrm{e})}.\tag{7}$$

由 Legendre 变换,广义位移的对偶变量为

$$\begin{cases}\boldsymbol{p}^{(\mathrm{PQC})}=\dfrac{\partial L^{(\mathrm{PQC})}}{\partial\dot{\boldsymbol{q}}^{(\mathrm{PQC})}}=\{r\sigma_{zr}^{(\mathrm{PQC})},rH_{zr}^{(\mathrm{PQC})},rD_r^{(\mathrm{PQC})}\}^{\mathrm{T}},\\ \boldsymbol{p}^{(\mathrm{PZC})}=\dfrac{\partial L^{(\mathrm{PZC})}}{\partial\dot{\boldsymbol{q}}^{(\mathrm{PZC})}}=\{r\sigma_{zr}^{(\mathrm{PZC})},rD_r^{(\mathrm{PZC})}\}^{\mathrm{T}},\ p^{(\mathrm{e})}=\dfrac{\partial L^{(\mathrm{e})}}{\partial\dot{\boldsymbol{q}}^{(\mathrm{e})}}=r\sigma_{zr}^{(\mathrm{e})}.\end{cases}\tag{8}$$

因此,Hamilton 函数为

$$H^{(i)}(\boldsymbol{q}^{(i)},\boldsymbol{p}^{(i)})=(\boldsymbol{p}^{(i)})^{\mathrm{T}}\dot{\boldsymbol{q}}^{(i)}-L_{\mathrm{QC}}(\boldsymbol{q}^{(i)},\dot{\boldsymbol{q}}^{(i)}).\tag{9}$$

由 Hamilton 变分原理,Hamilton 对偶方程为

$$\begin{Bmatrix}\dot{\boldsymbol{q}}^{(i)}\\ \dot{\boldsymbol{p}}^{(i)}\end{Bmatrix}=\begin{Bmatrix}\dfrac{\partial H^{(i)}}{\partial\boldsymbol{p}^{(i)}}\\ -\dfrac{\partial H^{(i)}}{\partial\boldsymbol{q}^{(i)}}\end{Bmatrix}=\begin{bmatrix}\boldsymbol{0} & \boldsymbol{M}^{(i)}\\ -\boldsymbol{M}^{(i)}\dfrac{\partial^2}{\partial\theta^2} & \boldsymbol{0}\end{bmatrix}\begin{Bmatrix}\boldsymbol{q}^{(i)}\\ \boldsymbol{p}^{(i)}\end{Bmatrix},\tag{10}$$

$$\boldsymbol{M}^{(\mathrm{PQC})}=\begin{bmatrix}C_{44}^{(\mathrm{PQC})} & R_3^{(\mathrm{PQC})} & e_{15}^{(\mathrm{PQC})}\\ R_3^{(\mathrm{PQC})} & K_2^{(\mathrm{PQC})} & d_{15}^{(\mathrm{PQC})}\\ e_{15}^{(\mathrm{PQC})} & d_{15}^{(\mathrm{PQC})} & -\lambda_{11}^{(\mathrm{PQC})}\end{bmatrix},\ \boldsymbol{M}^{(\mathrm{PZC})}=\begin{bmatrix}C_{44}^{(\mathrm{PZC})} & R_3^{(\mathrm{PZC})}\\ R_3^{(\mathrm{PZC})} & K_2^{(\mathrm{PZC})}\end{bmatrix}$$

为材料矩阵, $M^{(\mathrm{e})}=C_{44}^{(\mathrm{e})}$.

### 1.3　辛本征值和本征解

式(10)可采用分离变量法求解.令 $\boldsymbol{\psi}^{(i)}=\{\boldsymbol{q}^{(i)},\boldsymbol{p}^{(i)}\}\mathrm{e}^{-\mu\xi}$, 有

$$\begin{bmatrix}\boldsymbol{0} & \boldsymbol{M}^{(i)}\\ -\boldsymbol{M}^{(i)}\dfrac{\partial^2}{\partial\theta^2} & \boldsymbol{0}\end{bmatrix}\boldsymbol{\psi}^{(i)}=\mu\boldsymbol{\psi}^{(i)}. \tag{11}$$

式(11)有零本征值,其对应的本征解为

$$\begin{cases}\boldsymbol{\psi}_{01}^{(\mathrm{PQC})}=\{1,0,0,0,0,0\}^{\mathrm{T}},\\ \boldsymbol{\psi}_{02}^{(\mathrm{PQC})}=\{0,1,0,0,0,0\}^{\mathrm{T}},\\ \boldsymbol{\psi}_{03}^{(\mathrm{PQC})}=\{0,0,1,0,0,0\}^{\mathrm{T}},\end{cases}\begin{cases}\boldsymbol{\psi}_{01}^{(\mathrm{PZC})}=\{1,0,0,0\}^{\mathrm{T}},\\ \boldsymbol{\psi}_{02}^{(\mathrm{PZC})}=\{0,1,0,0\}^{\mathrm{T}},\end{cases}\boldsymbol{\psi}_{01}^{(\mathrm{e})}=\{1,0\}^{\mathrm{T}}. \tag{12}$$

对于非零本征值,式(11)的通解为

$$\boldsymbol{\psi}_n^{(i)}=\begin{bmatrix}\cos(\mu_n\theta)\boldsymbol{I}^{(i)} & \sin(\mu_n\theta)\boldsymbol{I}^{(i)}\\ \mu_n\cos(\mu_n\theta)\boldsymbol{M}^{(i)} & \mu_n\sin(\mu_n\theta)\boldsymbol{M}^{(i)}\end{bmatrix}\boldsymbol{x}_1^{(i)}, \tag{13}$$

其中 $\boldsymbol{x}_1^{(\mathrm{PQC})}=\{\chi_{11}^{(\mathrm{PQC})},\chi_{12}^{(\mathrm{PQC})},\chi_{13}^{(\mathrm{PQC})},\chi_{21}^{(\mathrm{PQC})},\chi_{22}^{(\mathrm{PQC})},\chi_{23}^{(\mathrm{PQC})}\}^{\mathrm{T}}$, $\boldsymbol{x}_1^{(\mathrm{PZC})}=\{\chi_{11}^{(\mathrm{PZC})},\chi_{12}^{(\mathrm{PZC})},\chi_{21}^{(\mathrm{PZC})},\chi_{22}^{(\mathrm{PZC})}\}^{\mathrm{T}}$, $\boldsymbol{x}_2^{(\mathrm{e})}=\{\chi_1^{(\mathrm{e})},\chi_2^{(\mathrm{e})}\}^{\mathrm{T}}$ 是未知系数,下标数字代表不同的子极坐标系; $\boldsymbol{I}^{(\mathrm{PQC})}$ 为三阶单位矩阵, $\boldsymbol{I}^{(\mathrm{PZC})}$ 为二阶单位矩阵, $I^{(\mathrm{e})}$ 为 1.式(13)在不同的子极坐标系下有着统一的形式,而未知系数在不同的子坐标系下有着不同的数值.这里以情况 1 为例,介绍未知系数的求解方法.

该情况下,上下切口面声子场、相位子场应力和电位移为零:

$$\{\sigma_{\theta z}|_{\theta=0},H_{z\theta}|_{\theta=0},D_\theta|_{\theta=0}\}^{\mathrm{T}}=\boldsymbol{0},\ \sigma_{\theta z}|_{\theta=-\gamma_1-\gamma_2-\gamma_3}=0. \tag{14}$$

压电准晶体与压电晶体界面处,声子场对应的应力、位移、电势和电位移连续,相位子场应力为零:

$$\begin{Bmatrix}\sigma_{\theta z}^{(\mathrm{PQC})}|_{\theta=-\gamma_1}\\ D_\theta^{(\mathrm{PQC})}|_{\theta=-\gamma_1}\end{Bmatrix}=\begin{Bmatrix}\sigma_{\theta z}^{(\mathrm{PZC})}|_{\theta=-\gamma_1}\\ D_\theta^{(\mathrm{PZC})}|_{\theta=-\gamma_1}\end{Bmatrix},\ \begin{Bmatrix}u_z^{(\mathrm{PQC})}|_{\theta=-\gamma_1}\\ \varphi^{(\mathrm{PQC})}|_{\theta=-\gamma_1}\end{Bmatrix}=\begin{Bmatrix}u_z^{(\mathrm{PZC})}|_{\theta=-\gamma_1}\\ \varphi^{(\mathrm{PZC})}|_{\theta=-\gamma_1}\end{Bmatrix},\ H_{z\theta}^{(\mathrm{PQC})}|_{\theta=-\gamma_1}=0. \tag{15}$$

压电晶体与弹性体界面处声子场应力、位移连续,电位移为零:

$$\sigma_{\theta z}^{(\mathrm{PZC})}|_{\theta=-\gamma_1-\gamma_2}=\sigma_{\theta z}^{(\mathrm{e})}|_{\theta=-\gamma_1-\gamma_2},\ u_z^{(\mathrm{PZC})}|_{\theta=-\gamma_1-\gamma_2}=u_z^{(\mathrm{e})}|_{\theta=-\gamma_1-\gamma_2},\ D_\theta^{(\mathrm{PZC})}|_{\theta=-\gamma_1-\gamma_2}=0. \tag{16}$$

将通解(13)代入边界条件(14)—(16)中可得

$$[-\sin(\mu_n\gamma_1)\boldsymbol{M}^{(\mathrm{PQC})}\quad\cos(\mu_n\gamma_1)\boldsymbol{M}^{(\mathrm{PQC})}]\boldsymbol{x}_1^{(\mathrm{PQC})}=0, \tag{17}$$

$$[\sin(\mu_n\gamma_3)C_{44}^{(\mathrm{e})}\quad\cos(\mu_n\gamma_3)C_{44}^{(\mathrm{e})}]\boldsymbol{x}_2^{(\mathrm{e})}=0, \tag{18}$$

$$[\boldsymbol{\Gamma}_1\quad\boldsymbol{0}_{2\times3}]\boldsymbol{x}_1^{(\mathrm{PQC})}=[\boldsymbol{I}^{(\mathrm{PZC})}\quad\boldsymbol{0}_{2\times2}]\boldsymbol{x}_1^{(\mathrm{PZC})}, \tag{19}$$

$$[\boldsymbol{0}_{2\times3}\quad\boldsymbol{\Gamma}_1\boldsymbol{M}^{(\mathrm{PQC})}]\boldsymbol{x}_1^{(\mathrm{PQC})}=[\boldsymbol{0}_{2\times2}\quad\boldsymbol{M}^{(\mathrm{PZC})}]\boldsymbol{x}_1^{(\mathrm{PZC})}, \tag{20}$$

$$[\boldsymbol{0}_{1\times3}\quad\boldsymbol{\Gamma}_2\boldsymbol{M}^{(\mathrm{PQC})}]\boldsymbol{x}_1^{(\mathrm{PQC})}=0, \tag{21}$$

$$[\boldsymbol{\Gamma}_3\quad\boldsymbol{0}_{1\times2}]\boldsymbol{x}_2^{(\mathrm{PZC})}=\boldsymbol{\Gamma}_3\boldsymbol{x}_2^{(\mathrm{e})}, \tag{22}$$

$$[\boldsymbol{0}_{1\times2}\quad\boldsymbol{\Gamma}_3\boldsymbol{M}^{(\mathrm{PZC})}]\boldsymbol{x}_2^{(\mathrm{PZC})}=[0\quad C_{44}^{(\mathrm{e})}]\boldsymbol{x}_2^{(\mathrm{e})}, \tag{23}$$

$$[\boldsymbol{0}_{1\times2}\quad\boldsymbol{\Gamma}_4\boldsymbol{M}^{(\mathrm{PZC})}]\boldsymbol{x}_2^{(\mathrm{PZC})}=0, \tag{24}$$

其中 $\boldsymbol{\Gamma}_1=\begin{bmatrix}1&0&0\\0&0&1\end{bmatrix}$, $\boldsymbol{\Gamma}_2=[0\quad1\quad0]$, $\boldsymbol{\Gamma}_3=[1\quad0]$, $\boldsymbol{\Gamma}_4=[0\quad1]$.

由于子坐标系 2 可以通过子坐标系 1 顺时针旋转 $\gamma_2$ 获得,因此, $\boldsymbol{x}_1^{(\mathrm{PZC})}$ 和 $\boldsymbol{x}_2^{(\mathrm{PZC})}$ 满足

$$\boldsymbol{x}_2^{(\mathrm{PZC})}=\begin{bmatrix}\cos(\mu_n\gamma_2)\boldsymbol{I}^{(\mathrm{PZC})} & -\sin(\mu_n\gamma_2)\boldsymbol{I}^{(\mathrm{PZC})}\\ \sin(\mu_n\gamma_2)\boldsymbol{I}^{(\mathrm{PZC})} & \cos(\mu_n\gamma_2)\boldsymbol{I}^{(\mathrm{PZC})}\end{bmatrix}\boldsymbol{x}_1^{(\mathrm{PZC})}. \tag{25}$$

因此,通解中的未知系数 $\boldsymbol{x}_1^{(i)}$ 和 $\boldsymbol{x}_2^{(i)}$ 满足

$$\boldsymbol{\Lambda}\{\boldsymbol{x}_1^{(\mathrm{PQC})},\boldsymbol{x}_1^{(\mathrm{PZC})},\boldsymbol{x}_2^{(\mathrm{e})}\}^{\mathrm{T}}=0, \tag{26}$$

其中 $\boldsymbol{\Lambda}$ 由式(17)—(25)获得.

式(26)有非零解,因此

$$|\boldsymbol{\Lambda}| = 0. \tag{27}$$

由于式(27)无法解析求解,采用迭代法可求出辛本征值的数值解.将本征值代入式(26)中,即可求出所有的非零本征值对应的本征解.至此,式(11)中的所有辛本征解已全部获得.因此,式(10)的解可以表达为这些辛本征解的线性组合:

$$\boldsymbol{\Psi}^{(i)} = \sum_{n=1}^{\infty} c_n \boldsymbol{\psi}_n^{(i)} r^{\mu_n}, \tag{28}$$

其中 $\boldsymbol{\psi}_n^{(i)}$ 为不同材料所对应的辛本征解, $c_n$ 为待定系数.

## 2 辛-等几何耦合方法

### 2.1 压电准晶体/压电晶体/弹性体的等几何列式

采用 NURBS 基函数对声子场/相位子场位移和电势进行离散:

$$u_z^{(i)} = \boldsymbol{R}(\zeta,\eta)\boldsymbol{u}_z^{(i)},\ w_z^{(i)} = \boldsymbol{R}(\zeta,\eta)\boldsymbol{w}_z^{(i)},\ \varphi^{(i)} = \boldsymbol{R}(\zeta,\eta)\boldsymbol{\varphi}^{(i)}, \tag{29}$$

其中 $\boldsymbol{u}_z^{(i)} = \{u_{z,11}^{(i)},\cdots,u_{z,kl}^{(i)},\cdots,u_{z,(p+1)(q+1)}^{(i)}\}^{\mathrm{T}}$, $\boldsymbol{w}_z^{(i)} = \{w_{z,11}^{(i)},\cdots,w_{z,kl}^{(i)},\cdots,w_{z,(p+1)(q+1)}^{(i)}\}^{\mathrm{T}}$ 和 $\boldsymbol{\varphi}^{(i)} = \{\varphi_{11}^{(i)},\cdots,\varphi_{kl}^{(i)},\cdots,\varphi_{(p+1)(q+1)}^{(i)}\}^{\mathrm{T}}$ 分别为控制点的未知量; $\boldsymbol{R}(\zeta,\eta) = \{R_{11}^{pq},\cdots,R_{kl}^{pq},\cdots,R_{(p+1)(q+1)}^{pq}\}$ 为双变量 NURBS 基函数向量; $\zeta$ 和 $\eta$ 为参数坐标; $p$ 和 $q$ 为 NURBS 基函数在不同方向的阶次.

对应声子场/相位子场应变和电场强度为

$$\{\gamma_{zx}^{(i)},\gamma_{zy}^{(i)}\}^{\mathrm{T}} = \boldsymbol{B}\boldsymbol{u}_z^{(i)},\ \{\omega_{zx}^{(i)},\omega_{zy}^{(i)}\}^{\mathrm{T}} = \boldsymbol{B}\boldsymbol{w}_z^{(i)},\ \{E_x^{(i)},E_y^{(i)}\}^{\mathrm{T}} = -\boldsymbol{B}\boldsymbol{\varphi}^{(i)}, \tag{30}$$

其中 $\boldsymbol{B} = \boldsymbol{J}_{\mathrm{c}}^{-1}\left[\dfrac{\partial \boldsymbol{R}^{\mathrm{T}}}{\partial\zeta},\dfrac{\partial \boldsymbol{R}^{\mathrm{T}}}{\partial\eta}\right]^{\mathrm{T}}$, $\boldsymbol{J}_{\mathrm{c}} = \begin{bmatrix} \dfrac{\partial x}{\partial\zeta} & \dfrac{\partial y}{\partial\zeta} \\ \dfrac{\partial x}{\partial\eta} & \dfrac{\partial y}{\partial\eta} \end{bmatrix}$.

将式(29)和(30)代入式(1)—(3)中,由变分原理即可得到等几何列式:

$$\boldsymbol{K}^{(i)}\boldsymbol{a}^{(i)} = \boldsymbol{P}^{(i)}, \tag{31}$$

其中 $\boldsymbol{a}^{(\mathrm{PQC})} = \{(\boldsymbol{u}_z^{(\mathrm{PQC})})^{\mathrm{T}},(\boldsymbol{w}_z^{(\mathrm{PQC})})^{\mathrm{T}},(\boldsymbol{\varphi}^{(\mathrm{PQC})})^{\mathrm{T}}\}^{\mathrm{T}}$, $\boldsymbol{a}^{(\mathrm{PZC})} = \{(\boldsymbol{u}_z^{(\mathrm{PZC})})^{\mathrm{T}},(\boldsymbol{\varphi}^{(\mathrm{PZC})})^{\mathrm{T}}\}^{\mathrm{T}}$ 和 $\boldsymbol{a}^{(\mathrm{e})} = \boldsymbol{u}_z^{(\mathrm{e})}$ 为控制点未知量向量.单元刚度阵 $\boldsymbol{K}^{(i)}$ 为

$$\boldsymbol{K}^{(\mathrm{PQC})} = \begin{bmatrix} \boldsymbol{K}_{uu}^{(\mathrm{PQC})} & \boldsymbol{K}_{uw}^{(\mathrm{PQC})} & \boldsymbol{K}_{u\varphi}^{(\mathrm{PQC})} \\ \boldsymbol{K}_{wu}^{(\mathrm{PQC})} & \boldsymbol{K}_{ww}^{(\mathrm{PQC})} & \boldsymbol{K}_{w\varphi}^{(\mathrm{PQC})} \\ \boldsymbol{K}_{\varphi u}^{(\mathrm{PQC})} & \boldsymbol{K}_{\varphi w}^{(\mathrm{PQC})} & \boldsymbol{K}_{\varphi\varphi}^{(\mathrm{PQC})} \end{bmatrix},\ \boldsymbol{K}^{(\mathrm{PZC})} = \begin{bmatrix} \boldsymbol{K}_{uu}^{(\mathrm{PZC})} & \boldsymbol{K}_{u\varphi}^{(\mathrm{PZC})} \\ \boldsymbol{K}_{\varphi u}^{(\mathrm{PZC})} & \boldsymbol{K}_{\varphi\varphi}^{(\mathrm{PZC})} \end{bmatrix},\ \boldsymbol{K}^{(\mathrm{e})} = \boldsymbol{K}_{uu}^{(\mathrm{e})}, \tag{32}$$

其中

$$\boldsymbol{K}_{uu}^{(i)} = \int_{\Omega}\boldsymbol{B}^{\mathrm{T}}C_{44}^{(i)}\boldsymbol{I}_{2\times2}\boldsymbol{B}\mathrm{d}\Omega,\ \boldsymbol{K}_{ww}^{(i)} = \int_{\Omega}\boldsymbol{B}^{\mathrm{T}}\boldsymbol{K}_2^{(i)}\boldsymbol{I}_{2\times2}\boldsymbol{B}\mathrm{d}\Omega,\ \boldsymbol{K}_{\varphi\varphi}^{(i)} = -\int_{\Omega}\boldsymbol{B}^{\mathrm{T}}\lambda_{11}^{(i)}\boldsymbol{I}_{2\times2}\boldsymbol{B}\mathrm{d}\Omega,$$

$$\boldsymbol{K}_{uw}^{(i)} = \boldsymbol{K}_{wu}^{(i)} = \int_{\Omega}\boldsymbol{B}^{\mathrm{T}}R_3^{(i)}\boldsymbol{I}_{2\times2}\boldsymbol{B}\mathrm{d}\Omega,\ \boldsymbol{K}_{u\varphi}^{(i)} = \boldsymbol{K}_{\varphi u}^{(i)} = \int_{\Omega}\boldsymbol{B}^{\mathrm{T}}e_{15}^{(i)}\boldsymbol{I}_{2\times2}\boldsymbol{B}\mathrm{d}\Omega,\ \boldsymbol{K}_{uw}^{(i)} = \boldsymbol{K}_{wu}^{(i)} = \int_{\Omega}\boldsymbol{B}^{\mathrm{T}}d_{15}^{(i)}\boldsymbol{I}_{2\times2}\boldsymbol{B}\mathrm{d}\Omega.$$

载荷向量 $\boldsymbol{P}^{(i)}$ 为

$$\boldsymbol{P}^{(\mathrm{PQC})} = \begin{Bmatrix} \boldsymbol{P}_u^{(\mathrm{PQC})} \\ \boldsymbol{P}_w^{(\mathrm{PQC})} \\ \boldsymbol{P}_\varphi^{(\mathrm{PQC})} \end{Bmatrix},\ \boldsymbol{P}^{(\mathrm{PZC})} = \begin{Bmatrix} \boldsymbol{P}_u^{(\mathrm{PZC})} \\ \boldsymbol{P}_\varphi^{(\mathrm{PZC})} \end{Bmatrix},\ \boldsymbol{P}^{(\mathrm{e})} = \boldsymbol{P}_u^{(\mathrm{e})}, \tag{33}$$

其中 $\boldsymbol{P}_u^{(i)} = \int_{\partial\Omega}\boldsymbol{R}^{\mathrm{T}}T_\sigma^{(i)}\mathrm{d}S$, $\boldsymbol{P}_w^{(i)} = \int_{\partial\Omega}\boldsymbol{R}^{\mathrm{T}}T_H^{(i)}\mathrm{d}S$, $\boldsymbol{P}_\varphi^{(i)} = \int_{\partial\Omega}\boldsymbol{R}^{\mathrm{T}}T_D^{(i)}\mathrm{d}S$.

### 2.2 压电准晶体/压电晶体/弹性体的辛-等几何耦合列式

将模型分为两个区域,如图 2 所示.$\Omega_{\mathrm{s}}$ 为奇异区,该区域受切口尖端的奇异应力影响较大.$\Omega_{\mathrm{n}}$ 为非奇异区,该区域远离切口尖端,受奇异应力影响较小.

将等几何列式(31)按奇异区和非奇异区进行分块:

$$\begin{bmatrix} \boldsymbol{K}_{\mathrm{ss}}^{(i)} & \boldsymbol{K}_{\mathrm{sn}}^{(i)} \\ \boldsymbol{K}_{\mathrm{ns}}^{(i)} & \boldsymbol{K}_{\mathrm{nn}}^{(i)} \end{bmatrix} \begin{Bmatrix} \boldsymbol{a}_{\mathrm{s}}^{(i)} \\ \boldsymbol{a}_{\mathrm{n}}^{(i)} \end{Bmatrix} = \begin{Bmatrix} \boldsymbol{P}_{\mathrm{s}}^{(i)} \\ \boldsymbol{P}_{\mathrm{n}}^{(i)} \end{Bmatrix}, \tag{34}$$

下标 s 和 n 代表奇异区和非奇异区.采用辛方法对奇异区进行求解,将奇异区的解式(28)代入式(34)中,即可获得辛-等几何耦合列式:

$$\begin{bmatrix} (\boldsymbol{\Phi}^{(i)})^{\mathrm{T}} \boldsymbol{K}_{\mathrm{ss}}^{(i)} \boldsymbol{\Phi}^{(i)} & \boldsymbol{K}_{\mathrm{sn}}^{(i)} \boldsymbol{\Phi}^{(i)} \\ (\boldsymbol{\Phi}^{(i)})^{\mathrm{T}} \boldsymbol{K}_{\mathrm{ns}}^{(i)} & \boldsymbol{K}_{\mathrm{nn}}^{(i)} \end{bmatrix} \begin{Bmatrix} \boldsymbol{c} \\ \boldsymbol{a}_{\mathrm{n}}^{(i)} \end{Bmatrix} = \begin{Bmatrix} (\boldsymbol{\Phi}^{(i)})^{\mathrm{T}} \boldsymbol{P}_{\mathrm{s}}^{(i)} \\ \boldsymbol{P}_{\mathrm{n}}^{(i)} \end{Bmatrix}, \tag{35}$$

其中 $\boldsymbol{\Phi}^{(i)}$ 由辛本征解组成.可以发现,辛-等几何耦合列式中,基本未知量为辛本征解的待定系数和非奇异区内控制点的未知量.当求解该方程,获得待定系数 $\boldsymbol{c}$, 即可获得模型奇异区内物理场的解析表达式.

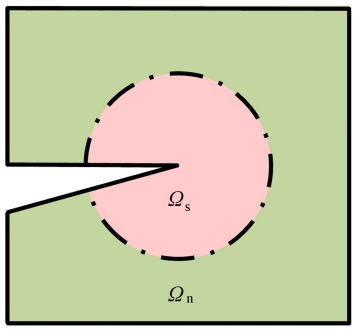


**图 2**　奇异区和非奇异区

Fig. 2　The singular region and the non-singular region

## 3　数值算例

为避免参与计算的矩阵奇异,对各材料参数和物理量无量纲化处理.材料参数为 $\bar{C}_{44} = C_{44}/(10^9\ \mathrm{Pa})$, $\bar{R}_3 = R_3/(10^9\ \mathrm{Pa})$, $\bar{K}_2 = K_2/(10^9\ \mathrm{Pa})$, $\bar{e}_{15} = e_{15}/(1\ \mathrm{C/m^2})$, $\bar{d}_{15} = d_{15}/(1\ \mathrm{C/m^2})$, $\bar{\lambda}_{11} = \lambda_{11} \times 10^9/(1\ \mathrm{C^2/(N\cdot m^2)})$; 位移和电势为 $\bar{u}_z = u_z/a$, $\bar{w}_z = w_z/a$, $\bar{\varphi} = \varphi \times (10^{-9}\ \mathrm{C/N})/a$; 应力和电位移为 $\bar{\sigma} = \sigma/(1\ \mathrm{GPa})$, $\bar{H} = H/(1\ \mathrm{GPa})$, $\bar{D} = D/(1\ \mathrm{C/m^2})$; 外加载荷为 $\bar{F}_\sigma = F_\sigma/(10^9\ \mathrm{N})$, $\bar{F}_H = F_H/(10^9\ \mathrm{N})$, $\bar{Q} = Q/(1\ \mathrm{C})$.采用的材料参数[22,24-25]如表 1 所示.

**表 1**　压电准晶体/压电晶体/弹性体材料参数

Table 1　The material constants of PQC/PZC/elastic materials

| | $C_{44}$ /GPa | $R_3$ /GPa | $K_2$ /GPa | $e_{15}$ /(C/m$^2$) | $d_{15}$ /(C/m$^2$) | $\lambda_{11}$ /(C$^2$/(N·m$^2$)) |
|---|---|---|---|---|---|---|
| PQC | 50 | 1.2 | 0.18 | −0.138 | −0.16 | $8.26\times10^{-11}$ |
| PZC | 25.6 | – | – | 12.7 | – | 6.46 |
| epoxy | 1.76 | – | – | – | – | – |

### 3.1　对比算例

由于目前尚未有针对含有切口的压电准晶体/压电晶体/弹性体三材料结构断裂问题的研究,为验证提出方法的正确性,首先考虑如图 3 所示的含中心裂纹的单一压电准晶体模型.其边界受均布反对称荷载作用: $\bar{\sigma}_0 = \bar{H}_0 = \bar{D}_0 = 1$, 模型的几何参数为 $W = H = L$, $\delta_1 = W/2 - a$, $\delta_2 = H/2$.

图 4 展示了不同位置裂纹对应的应力强度因子随边长的变化曲线.由于模型和载荷对称,三场的强度因子相等,即: $K_{\mathrm{III}}^{\sigma} = K_{\mathrm{III}}^{H} = K_{\mathrm{III}}^{D} = K_{\mathrm{III}}^{*}$.从图中可以发现,随着模型尺寸增加,应力强度因子不断变小,最终收敛于一个常数,该常数与无限大模型所对应的解析解[26]一致.

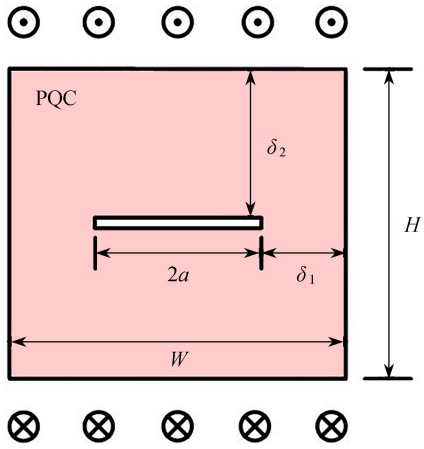


**图 3**　含内部裂纹的压电准晶体

Fig. 3　The square PQC with an internal crack

为进一步验证所提出的方法,将三材料模型中的压电准晶体的相位子场进行退化,考虑一个如图 5 所示的含有边裂纹的圆形压电晶体/环氧树脂组合模型,其上下边界受反对称集中荷载 $\bar{F}_\sigma = 1$, 模型上边界和双材料界面接地.计算参数为 $\gamma = \pi/2$. Mat-1 为压电晶体材料,其材料参数为 $\tilde{C}_{44}^{(\mathrm{PZC})} = \kappa_1 C_{44}^{(\mathrm{PZC})}$, $\tilde{e}_{15}^{(\mathrm{PZC})} = \kappa_2 e_{15}^{(\mathrm{PZC})}$, $\tilde{\lambda}_{11}^{(\mathrm{PZC})} = \kappa_3 \lambda_{11}^{(\mathrm{PZC})}$; Mat-2 为弹性体,其材料参数为 $C_{44}^{(\mathrm{e})}$.其中, $e_{15}^{(\mathrm{PZC})}$ 和 $C_{44}^{(\mathrm{e})}$ 取表 1 中的参数.图 6 显示了不同材料参数 ($\kappa_1$, $\kappa_2$, $\kappa_3$) 下三场的应

力强度因子.从图中曲线可以发现,辛-等几何耦合方法所得结果与文献[22]吻合良好,进一步验证了本文方法的准确性.此外,图中曲线还表明,该情况下不同材料参数对各场强度因子影响不同,并且主要影响电位移强度因子.

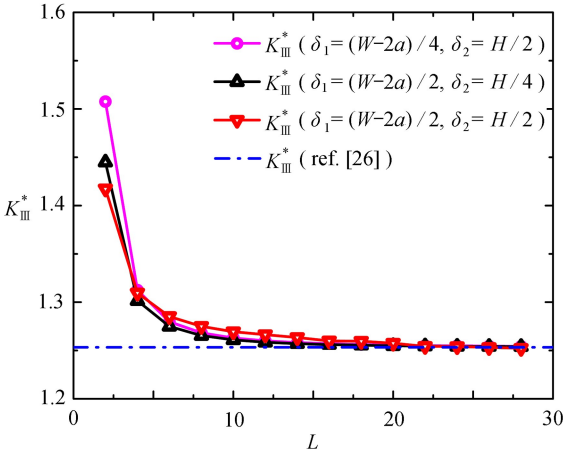


**图 4** 应力强度因子随模型尺寸的变化

Fig. 4 The variations of the stress intensity factor vs. the size of the model

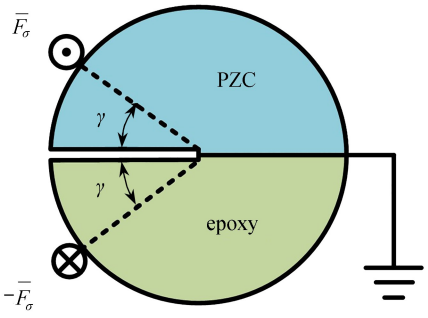


**图 5** 圆形压电晶体/环氧树脂双材料结构

Fig. 5 The circular PZC/epoxy bi-material

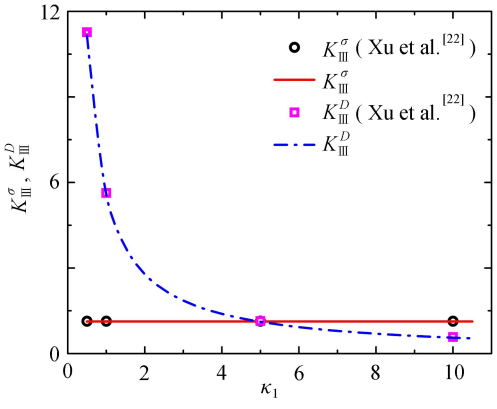


(a) $\kappa_1$ 的影响

(a) The effects of $\kappa_1$

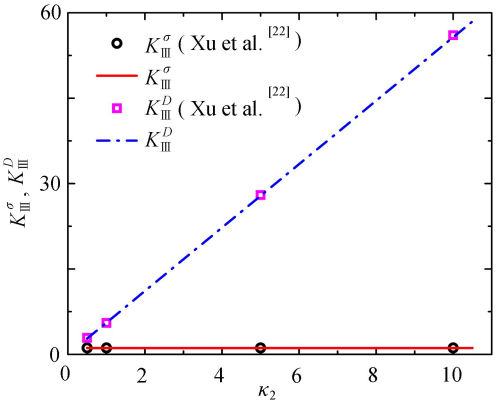


(b) $\kappa_2$ 的影响

(b) The effects of $\kappa_2$

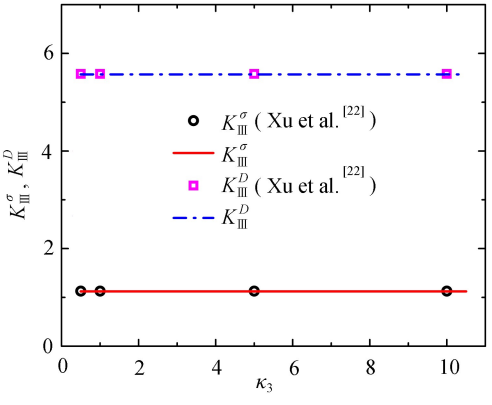


(c) $\kappa_3$ 的影响

(c) The effects of $\kappa_3$

**图 6** 材料参数对应力、电位移强度因子的影响

Fig. 6 The effects of the material constants on the stress and electric displacement intensity factors

### 3.2　压电准晶体/压电晶体/弹性体三材料结构的奇异性

考虑图 1 中各角度对切口尖端奇异性的影响.计算参数为 $\gamma_1=\gamma_3=\Delta\theta,\gamma_2=180°$.表 2—4 给出了不同情况下,切口尖端的奇异性随各角度的变化.结果显示情况 1 和情况 2 均有两个奇异性指数,而情况 3 仅有一个奇异性指数,并且所有的奇异性指数均随着角度 $\Delta\theta$ 的增加而降低.因此,切口的角度越小,3 种情况的应力奇异性越强.

**表 2**　情况 1 时切口奇异性指数随角度 $\Delta\theta$ 的变化

Table 2　The variations of the singularity orders vs. $\Delta\theta$ in case 1

| | $\Delta\theta$ | | | | |
|---|---|---|---|---|---|
| | 50° | 60° | 70° | 80° | 90° |
| $\mu_1-1$ | −0.209 8 | −0.243 8 | −0.275 9 | −0.306 0 | −0.334 5 |
| $\mu_2-1$ | −0.013 2 | −0.018 8 | −0.028 0 | −0.046 2 | −0.083 7 |

**表 3**　情况 2 时切口奇异性指数随角度 $\Delta\theta$ 的变化

Table 3　The variations of the singularity orders vs. $\Delta\theta$ in case 2

| | $\Delta\theta$ | | | | |
|---|---|---|---|---|---|
| | 50° | 60° | 70° | 80° | 90° |
| $\mu_1-1$ | −0.476 8 | −0.481 0 | −0.484 2 | −0.486 7 | −0.488 7 |
| $\mu_2-1$ | −0.240 0 | −0.273 6 | −0.304 1 | −0.332 5 | −0.358 0 |

**表 4**　情况 3 时切口奇异性指数随角度 $\Delta\theta$ 的变化

Table 4　The variations of the singularity orders vs. $\Delta\theta$ in case 3

| | $\Delta\theta$ | | | | |
|---|---|---|---|---|---|
| | 50° | 60° | 70° | 80° | 90° |
| $\mu_1-1$ | −0.838 9 | −0.852 8 | −0.863 6 | −0.872 4 | −0.879 7 |

### 3.3　含边切口的方形三材料结构

考虑如图 7 所示的含有边切口的方形压电准晶体/压电晶体/环氧树脂组合结构,分别考虑情况 1、情况 2、情况 3 三种组合方式.三材料角度分别为: $\gamma_1=\gamma_3=60°$ 和 $\gamma_2=180°$;切口深度为 $a$;模型宽和高为 $L=6$, $H=12$;无量纲载荷参数为:$\Delta u=\Delta w=\Delta\varphi=0.1$.由于三材料组合结构尖端奇异性指数不再为−1/2,这里采用文献[23,27]所定义的广义强度系数.

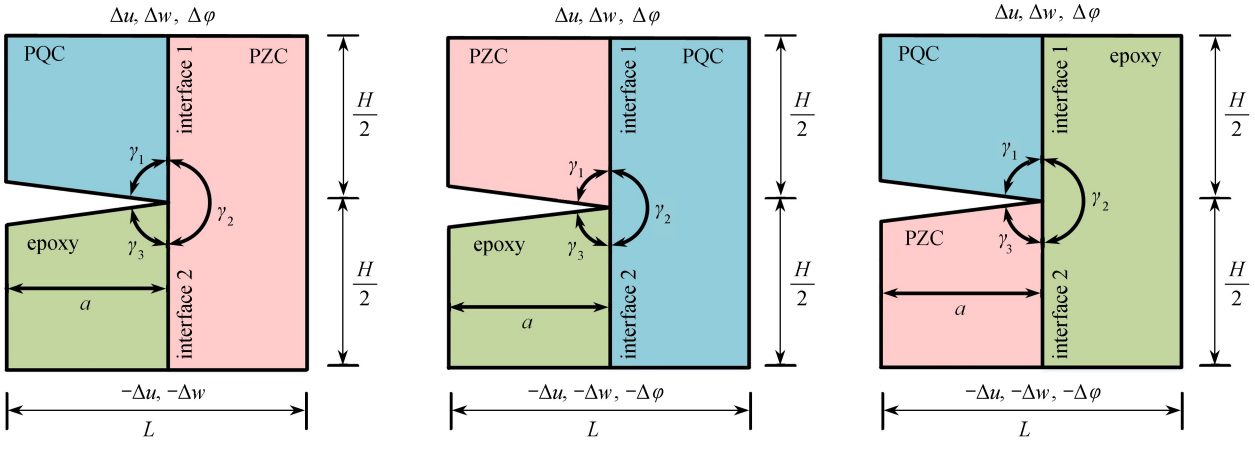


(a) 情况 1　(b) 情况 2　(c) 情况 3

(a) Case 1　(b) Case 2　(c) Case 3

**图 7**　含边切口的方形压电准晶体/压电晶体/环氧树脂模型

Fig. 7　The square PQC/PZC/epoxy composite models

表 5—10 为三场强度系数.结果发现,在情况 1 下,切口有两个奇异本征值;界面 1 有电位移强度系数,界面 2 无电位移强度系数;并且两个界面上 $K_{\mathrm{I}}^{\sigma}$ 占主导.情况 2 下,切口仍有两个奇异本征值;界面 1 有电位

移强度系数,界面 2 无电位移强度系数;两个界面上 $K_2^\sigma$ 占主导.情况 3 下,切口仅有一项奇异本征值,此时双界面上均只有声子场应力强度系数.

**表 5** 界面 1 强度系数(情况 1)

Table 5 The intensity coefficients at interface 1 (case 1)

| | $a$ | | | | |
|---|---|---|---|---|---|
| | 1 | 2 | 3 | 4 | 5 |
| $K_1^\sigma$ | 0.949 0 | 1.042 3 | 1.058 4 | 1.049 7 | 1.023 7 |
| $K_1^D$ | 0.011 0 | 0.012 0 | 0.012 2 | 0.012 1 | 0.011 8 |
| $K_1^H$ | 0 | 0 | 0 | 0 | 0 |
| $K_2^\sigma$ | −0.021 3 | −0.021 5 | −0.021 6 | −0.021 6 | −0.021 6 |
| $K_2^D$ | 0.010 9 | 0.011 0 | 0.011 0 | 0.011 0 | 0.011 0 |
| $K_2^H$ | 0 | 0 | 0 | 0 | 0 |

**表 6** 界面 2 强度系数(情况 1)

Table 6 The intensity coefficients at interface 2 (case 1)

| | $a$ | | | | |
|---|---|---|---|---|---|
| | 1 | 2 | 3 | 4 | 5 |
| $K_1^\sigma$ | 0.051 2 | 0.056 3 | 0.057 1 | 0.056 7 | 0.055 3 |
| $K_1^D$ | 0 | 0 | 0 | 0 | 0 |
| $K_2^\sigma$ | 0.000 9 | 0.000 9 | 0.000 9 | 0.000 9 | 0.000 9 |
| $K_2^D$ | 0 | 0 | 0 | 0 | 0 |

**表 7** 界面 1 强度系数(情况 2)

Table 7 The intensity coefficients at interface 1 (case 2)

| | $a$ | | | | |
|---|---|---|---|---|---|
| | 1 | 2 | 3 | 4 | 5 |
| $K_1^\sigma$ | −0.014 5 | −0.014 4 | −0.014 0 | −0.012 8 | −0.009 9 |
| $K_1^D$ | 0.007 9 | 0.007 8 | 0.007 6 | 0.007 0 | 0.005 4 |
| $K_1^H$ | 0 | 0 | 0 | 0 | 0 |
| $K_2^\sigma$ | 0.932 9 | 1.028 9 | 1.044 1 | 1.031 7 | 0.994 9 |
| $K_2^D$ | 0.011 7 | 0.012 9 | 0.013 1 | 0.013 0 | 0.012 5 |
| $K_2^H$ | 0 | 0 | 0 | 0 | 0 |

**表 8** 界面 2 强度系数(情况 2)

Table 8 The intensity coefficients at interface 2 (case 2)

| | $a$ | | | | |
|---|---|---|---|---|---|
| | 1 | 2 | 3 | 4 | 5 |
| $K_1^\sigma$ | 0.000 4 | 0.000 4 | 0.000 4 | 0.000 4 | 0.000 3 |
| $K_1^D$ | 0 | 0 | 0 | 0 | 0 |
| $K_1^H$ | 0 | 0 | 0 | 0 | 0 |
| $K_2^\sigma$ | 0.048 9 | 0.053 9 | 0.054 7 | 0.054 1 | 0.052 1 |
| $K_2^D$ | 0 | 0 | 0 | 0 | 0 |
| $K_2^H$ | 0 | 0 | 0 | 0 | 0 |

**表 9** 界面 1 强度系数(情况 3)

Table 9 The intensity coefficients at interface 1 (case 3)

| | $a$ | | | | |
|---|---|---|---|---|---|
| | 1 | 2 | 3 | 4 | 5 |
| $K_1^\sigma$ | 0.058 0 | 0.075 1 | 0.076 0 | 0.073 6 | 0.073 6 |
| $K_1^D$ | 0 | 0 | 0 | 0 | 0 |
| $K_1^H$ | 0 | 0 | 0 | 0 | 0 |

**表 10**　界面 2 强度系数(情况 3)

Table 10　The intensity coefficients at interface 2 (case 3)

| | $a$ | | | | |
|---|---|---|---|---|---|
| | 1 | 2 | 3 | 4 | 5 |
| $K_{\mathrm{I}}^{\sigma}$ | 0.058 3 | 0.075 4 | 0.076 4 | 0.074 0 | 0.074 0 |
| $K_{\mathrm{I}}^{D}$ | 0 | 0 | 0 | 0 | 0 |

# 4　结　　论

本文发展了一种适用于压电准晶多材料组合结构界面断裂问题的辛-等几何耦合方法.该方法可以分析含 V 形切口的压电准晶体/压电晶体/弹性体的界面断裂问题,直接获得切口尖端附近区域内的奇异物理场的解析表达式以及各物理场对应的强度因子.该方法克服了传统数值方法在计算强度因子时存在网格和路径依赖问题,并且不需要引入新的单元和复杂的后处理程序.

**参考文献**(References):


[1] DING D H, YANG W G, HU C Z, et al. Generalized elasticity theory of quasi-crystals[J]. *Physical Review B*, 1993, **48**(10): 7003-7010.

[2] LI X F, FAN T Y, SUN Y F. A decagonal quasicrystal with a Griffith crack[J]. *Philosophical Magazine A*, 1999, **79**(8): 1943-1952.

[3] FAN T Y, MAI Y W. Elasticity theory, fracture mechanics, and some relevant thermal properties of quasi-crystalline materials[J]. *Applied Mechanics Reviews*, 2004, **57**(5): 325-343.

[4] GUO J H, YU J, XING Y M. Anti-plane analysis on a finite crack in a one-dimensional hexagonal quasicrystal strip[J]. *Mechanics Research Communications*, 2013, **52**: 40-45.

[5] LI L H, LIU G T. Icosahedral quasicrystals solids with an elliptic hole under uniform heat flow[J]. *Chinese Physics B*, 2014, **23**(5): 056101.

[6] 苏梦雨, 肖俊华, 冯国益. 一维六方准晶中纳米尺度开裂孔洞的Ⅲ型断裂力学[J]. 固体力学学报, 2020, **41**(3): 281-292. (SU Mengyu, XIAO Junhua, FENG Guoyi. Type Ⅲ fracture mechanics of a nanoscale cracked hole in one-dimensional hexagonal quasicrystal[J]. *Chinese Journal of Solid Mechanics*, 2020, **41**(3): 281-292. (in Chinese))

[7] 范天佑. 准晶数学弹性力学和缺陷力学[J]. 力学进展, 2000, **30**(2): 161-174. (FAN Tianyou. Mathematical theory of elasticity and defects of quasicrystals[J]. *Advances in Mechanics*, 2000, **30**(2): 161-174. (in Chinese))

[8] GAO Y, RICOEUR A, ZHANG L L, et al. Crack solutions and weight functions for plane problems in three-dimensional quasicrystals[J]. *Archive of Applied Mechanics*, 2014, **84**(8): 1103-1115.

[9] WANG X, SCHIAVONE P. Elastic field for a blunt crack in a decagonal quasicrystalline material[J]. *Engineering Fracture Mechanics*, 2019, **220**: 106657.

[10] HU K, YANG W, FU J, et al. Analysis of an anti-plane crack in a one-dimensional orthorhombic quasicrystal strip[J]. *Mathematics and Mechanics of Solids*, 2022,**27**(11): 2467-2479.

[11] LI L H, LIU G T. Decagonal quasicrystal plate with elliptic holes subjected to out-of-plane bending moments [J]. *Physics Letters A*, 2014, **378**(10): 839-844.

[12] 张炳彩, 丁生虎, 张来萍. 一维六方准晶双材料中圆孔边共线界面裂纹的反平面问题[J]. 应用数学和力学, 2022, **43**(6): 639-647. (ZHANG Bingcai, DING Shenghu, ZHANG Laiping. The anti-plane problem of collinear interface cracks emanating from a circular hole in 1D hexagonal quasicrystal bi-materials[J]. *Applied Mathematics and Mechanics*, 2022, **43**(6): 639-647. (in Chinese))

[13] 卢绍楠, 赵雪芬, 马园园. 一维六方压电准晶双材料界面共线裂纹问题[J]. 应用数学和力学, 2023, **44**(7): 809-824. (LU Shaonan, ZHAO Xuefen, MA Yuanyuan. Research on interfacial collinear cracks between 1D hexagonal piezoelectric quasicrystal bimaterials[J]. *Applied Mathematics and Mechanics*, 2023, **44**(7): 809-824. (in Chinese))

[14] JIANG L J, LIU G T. The interaction between a screw dislocation and a wedge-shaped crack in one-dimensional hexagonal piezoelectric quasicrystals[J]. *Chinese Physics B*, 2017, **26**(4): 044601.

[15] LI Y D, BAO R, CHEN W. Axial shear fracture of a transversely isotropic piezoelectric quasicrystal cylinder: which field (phonon or phason) has more contribution? [J]. *European Journal of Mechanics A: Solids*, 2018, **71**: 179-186.

[16] ZHOU Y B, LI X F. Fracture analysis of an infinite 1D hexagonal piezoelectric quasicrystal plate with a penny-shaped dielectric crack[J]. *European Journal of Mechanics A: Solids*, 2019, **76**: 224-234.

[17] ZHAO M, DANG H, FAN C, et al. Analysis of a three-dimensional arbitrarily shaped interface crack in a one-dimensional hexagonal thermo-electro-elastic quasicrystal bi-material, part 1: theoretical solution[J]. *Engineering Fracture Mechanics*, 2017, **179**: 59-78.

[18] DANG H, ZHAO M, FAN C, et al. Analysis of a three-dimensional arbitrarily shaped interface crack in a one-dimensional hexagonal thermo-electro-elastic quasicrystal bi-material, part 2: numerical method[J]. *Engineering Fracture Mechanics*, 2017, **180**: 268-281.

[19] HU K, GAO C, ZHONG Z, et al. Interaction of collinear interface cracks between dissimilar one-dimensional hexagonal piezoelectric quasicrystals[J]. *ZAMM-Journal of Applied Mathematics and Mechanics/Zeitschrift für Angewandte Mathematik und Mechanik*, 2021, **101**(11): e202000360.

[20] HUGHES T J R, COTTRELL J A, BAZILEVS Y. Isogeometric analysis: CAD, finite elements, NURBS, exact geometry and mesh refinement[J]. *Computer Methods in Applied Mechanics and Engineering*, 2005, **194**(39): 4135-4195.

[21] 姚伟岸, 钟万勰. 辛弹性力学[M]. 北京: 高等教育出版社, 2002. (YAO Weian, ZHONG Wanxie. *Symplectic Elasticity*[M]. Beijing: Higher Education Press, 2002. (in Chinese))

[22] XU C H, ZHOU Z H, XU X S, et al. Electroelastic singularities and intensity factors for an interface crack in piezoelectric-elastic bimaterials[J]. *Applied Mathematical Modelling*, 2015, **39**(9): 2721-2739.

[23] ZHOU Z, YANG Z, XU W, et al. Evaluation of electroelastic singularity of finite-size V-notched one-dimensional hexagonal quasicrystalline bimaterials with piezoelectric effect[J]. *Theoretical and Applied Fracture Mechanics*, 2019, **100**: 139-153.

[24] WU Y F, CHEN W Q, LI X Y. Indentation on one-dimensional hexagonal quasicrystals: general theory and complete exact solutions[J]. *Philosophical Magazine*, 2013, **93**(8): 858-882.

[25] LI X Y, LI P D, WU T H, et al. Three-dimensional fundamental solutions for one-dimensional hexagonal quasicrystal with piezoelectric effect[J]. *Physics Letters A*, 2014, **378**(10): 826-834.

[26] YANG J, LI X. Analytic solutions of problem about a circular hole with a straight crack in one-dimensional hexagonal quasicrystals with piezoelectric effects[J]. *Theoretical and Applied Fracture Mechanics*, 2016, **82**: 17-24.

[27] CHEN C D, CHUE C H. Singular electro-mechanical fields near the apex of a piezoelectric bonded wedge under antiplane shear[J]. *International Journal of Solids and Structures*, 2003, **40**(23): 6513-6526.